Am J Physiol Renal Physiol 323: F198–F211, 2022.
First published July 7, 2022; doi:10.1152/ajprenal.00005.2022

american physiological society

AMERICAN JOURNAL OF PHYSIOLOGY
RENAL PHYSIOLOGY

RESEARCH ARTICLE

Molecular Basis of Kidney Injury and Repair

Kidney-targeted irradiation triggers renal ischemic preconditioning in mice

Badr Khbouz,[1,9] François Lallemand,[2,3] Arianna Cirillo,[7] Pascal Rowart,[1,4] David Legouis,[5,8] Nor Eddine Sounni,[6] Agnès Noël,[6] Pascal De Tullio,[7] Sophie de Seigneux,[8] and François Jouret[1,9]

[1]*Groupe Interdisciplinaire de Génoprotéomique Appliquée, Cardiovascular Sciences, University of Liège, Liège, Belgium;* [2]*Cyclotron Research Center, University of Liège, Liège, Belgium;* [3]*Division of Radiotherapy, CHU of Liège, University of Liège, Liège, Belgium;* [4]*Department of Pharmacology and Chemical Biology, School of Medicine, University of Pittsburgh, Pittsburgh, Pennsylvania;* [5]*Division of Intensive Care, Department of Acute Medicine, Geneva University Hospitals, Geneva, Switzerland;* [6]*Groupe Interdisciplinaire de Génoprotéomique Appliquée, Cancer Sciences, University of Liège, Liège, Belgium;* [7]*Center for Interdisciplinary Research on Medicines, Metabolomics Group, University of Liège, Liège, Belgium;* [8]*Laboratory of Nephrology, Department of Medicine and Cell Physiology, University Hospital and University of Geneva, Geneva, Switzerland; and* [9]*Division of Nephrology, CHU of Liège, University of Liège, Liège, Belgium*

Abstract

Renal ischemia-reperfusion (I/R) causes acute kidney injury (AKI). Ischemic preconditioning (IPC) attenuates I/R-associated AKI. Whole body irradiation induces renal IPC in mice. Still, the mechanisms remain largely unknown. Furthermore, the impact of kidney-centered irradiation on renal resistance against I/R has not been studied. Renal irradiation (8.5 Gy) was done in male 8- to 12-wk-old C57bl/6 mice using a small animal radiation therapy device. Left renal I/R was performed by clamping the renal pedicles for 30 min, with simultaneous right nephrectomy, at 7, 14, and 28 days postirradiation. The renal reperfusion lasted 48 h. Following I/R, blood urea nitrogen (BUN) and serum creatinine (SCr) levels were lower in preirradiated mice compared with controls; so was the histological Jablonski score of AKI. The metabolomics signature of renal I/R was attenuated in preirradiated mice. The numbers of proliferating cell nuclear antigen (PCNA)-, cluster of differentiation molecule 11b (CD11b)-, and cell surface glycoprotein F4/80-positive cells in the renal parenchyma post-I/R were reduced in preirradiated versus control groups. Such IPC was significantly observed as early as *day 14* postirradiation. RNA sequencing showed an upregulation of angiogenesis- and stress response-related signaling pathways in irradiated nonischemic kidneys on *day 28*. Qualitative RT-PCR confirmed the increased expression of vascular endothelial growth factor (*VEGF*), activin receptor-like kinase 5 (*ALK5*), heme oxygenase-1 (*HO1*), platelet endothelial cell adhesion molecule-1 (*PECAM1*), NADPH oxidase 2 (*NOX2*), and heat shock proteins 70 and 27 (*HSP70* and *HSP27*, respectively) in irradiated kidneys compared with controls. In addition, irradiated kidneys showed an increased CD31-positive vascular area compared with controls. A 14-day gavage of irradiated mice with the antiangiogenic drug sunitinib before I/R abrogated the irradiation-induced IPC at both functional and structural levels. Our observations suggest that kidney-centered irradiation activates proangiogenic pathways and induces IPC, with preserved renal function and attenuated inflammation post-I/R.

NEW & NOTEWORTHY This study based on a mouse model of renal ischemia-reperfusion (I/R) aimed to *1*) test whether and how irradiation strictly centered on the kidney protects against the I/R injury and *2*) determine the shortest efficient delay of kidney irradiation to achieve such nephroprotection. Kidney irradiation increased the vascular surface in the renal parenchyma and conferred resistance against renal I/R damage, which highlights novel putative strategies in the field of ischemic acute kidney injury.

acute kidney injury; radiotherapy; renal ischemia-reperfusion; renal preconditioning; transcriptomics

INTRODUCTION

Acute kidney injury (AKI) is a commonly encountered syndrome associated with various pathophysiological processes leading to an abrupt decrease in kidney functions (1). AKI affects ~1,000 people per million and is associated with a high mortality rate (2). Renal ischemia-reperfusion (I/R) injury is the leading cause of AKI (3) and is induced by the transient interruption of renal blood flow that produces an abrupt drop in oxygen pressure and nutrient delivery leading to vascular and tubular dysfunction (4–6) and renal inflammation (7). I/R is an unavoidable event in kidney transplantation

Correspondence: F. Jouret (francois.jouret@chuliege.be).
Submitted 22 February 2022 / Revised 2 June 2022 / Accepted 27 June 2022

and cardiothoracic surgery, with a negative impact on short- and long-term kidney outcomes (8, 9). In the absence of specific pharmacological targets, the current (preventive and curative) management of I/R injury remains largely supportive (10). Translational research in the field focuses on the pathophysiology of renal ischemic preconditioning (IPC) to refine strategies for preventing or attenuating the severity of AKI and improving patients' health and survival (11, 12).

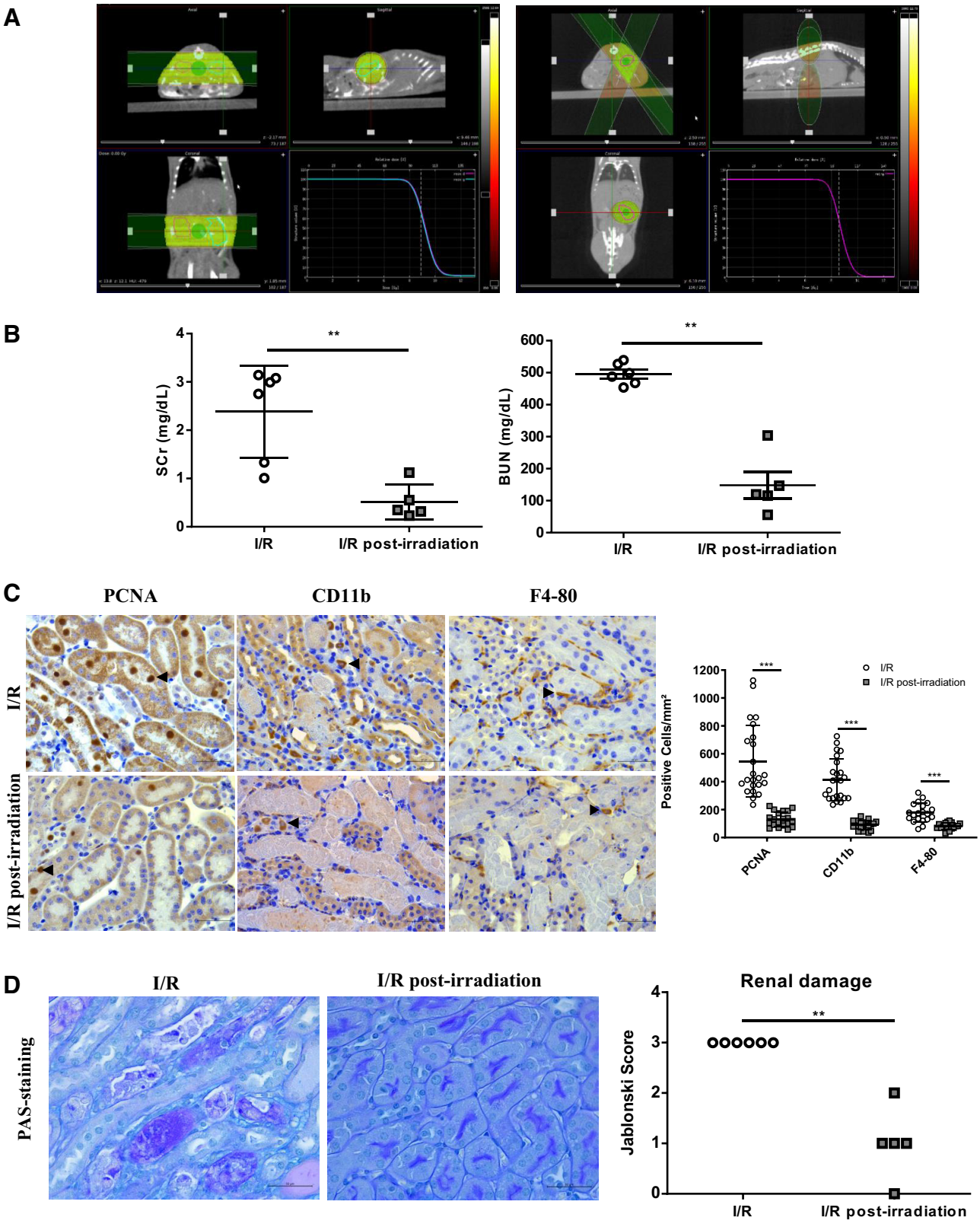

Several studies have reported a protective effect of radiation therapy against I/R injury. Yuan- Po et al. (13) showed that far-infrared radiation attenuated I/R injury in the rat testis by inducing heme oxygenase-1 (HO1) expression. Lakyova et al. (14) similarly demonstrated that low-level laser irradiation causes a profound reduction in the amount of necrotic tissue and enhances recovery after I/R muscle injury in rat hindlimbs by attenuating the inflammatory reaction and facilitating angiogenesis. In the global context of kidney diseases, it has been shown that continuous whole body low-dose-rate γ-irradiation ameliorates diabetic nephropathy and increases lifespan in mice through the activation of renal antioxidants (15). Taylor et al. (16) also showed that the incidence of kidney disease was significantly reduced in mice following irradiation compared with nonirradiated controls. Interestingly enough, in the context of in vivo studies of renal I/R, whole body irradiation has been suggested to induce renal IPC in mice. Indeed, 8-Gy whole body irradiation significantly attenuated the elevations of serum creatinine (SCr) and blood urea nitrogen (BUN) as well as structural damage and lipid peroxidation following renal I/R (17). However, the effect of irradiation focused specifically on the kidneys has never been evaluated, and the mechanisms of irradiation-induced IPC remain largely unknown.

Advances in conformational radiology and preclinical radiotherapy research have recently spurred the development of precise microirradiators for small animals, including rodents. These devices are often kilovolt X-ray radiation sources combined with high-resolution computed tomography (CT) imaging equipment for image guidance, as the latter allows precise and accurate beam positioning. These devices are similar to modern human radiotherapy machines and are considered a major step forward in radiobiology research (18, 19).

In the present study, we used the small animal radiation therapy with advanced precision (SmART), a well-validated preclinical microirradiator effective in the precise targeting of a specific organ in rodents (20). To our knowledge, we demonstrated, for the first time, that kidney-centered irradiation is associated with renal angiogenesis and renal IPC, with preserved renal function and attenuated renal inflammation post-I/R.

MATERIALS AND METHODS

Mouse Model of Renal I/R

The Institutional Animal Care and Use Committee of the University of Liege approved the present protocols (Nos. 1335 and 2185). All mice were housed in ventilated cages under conditions of stable temperature (23°C) and humidity under a dark-light cycle, with ad libitum access to food and water. All recordings/analyses were carried out by investigators who were blinded to the experimental conditions. Male C57bl/6 mice aged 8–12 wk (~26 g) were anesthetized with pentobarbital (60 mg/kg). Analgesia was performed preoperatively using buprenorphine (0.05 mg/kg). Median laparotomy was performed on heating pads, and a vascular clamp was applied for 30 min on the left renal pedicle. The right kidney was removed during the ischemia time and was half-cut to be fixed in paraformaldehyde or snap-frozen in liquid nitrogen. During the laparotomy, mice were covered with moistened gauze, and saline solution (0.5 mL/100 g), and antibiotics [Enrofloxacin (2.5%), 0.025 mL/mouse] were intraperitoneally infused. After surgery, mice were monitored twice daily. The left kidney was reperfused for 48 h. Mice were then anesthetized. A blood sample was collected by puncture of the inferior vena cava and centrifuged at 100 *g* for 10 min at 4°C. Serum levels of SCr and BUN were measured by enzymatic methods (Roche/Hitachi Cobas). The left kidney was excised, half-cut, and fixed in paraformaldehyde or snap-frozen in liquid nitrogen.

Animal Radiation Therapy

Mice were anesthetized with 4% isoflurane and maintained asleep by 1.5% isoflurane on the platform of the CT scanner with their head inserted into a 10-mL syringe connected to the isoflurane supply. We used a small animal irradiator and scanner (SmART) instrument from precision X-Ray (North Branford, CT) designed to image, target, and irradiate cells and small animals up to the size of rodents (see https://precisionxray.com/small-animal-igrt/). This scanner provides images that have a resolution of 0.1 mm. A prescan of the whole body was initially carried out to locate more precisely the volume to be investigated, and this volume was then defined in all three dimensions by moving cursors on the computer screen with the mouse. The acquisition scan was then started after adjusting parameters to 40 Kv, 8 mA, and a voxel resolution of 0.1 × 0.1 × 0.1 mm. We then performed the radiation therapy focused on the kidneys, with beams of 225 Kv and 13 mA. For bilateral irradiation, two opposite beams of X-rays targeted both kidneys to deliver a dose of 8.5 Gy. For unilateral irradiation, three opposite beams of X-rays were performed targeting one kidney to deliver a dose of 8.5 Gy (Fig. 1*A*). Mice were then placed in a recovery cage lightly heated by a lamp for recovery within minutes.

Figure 1. *A*: PXi X-Rad small animal radiation therapy with advanced precision renal radiation therapy. *A*, *left*: bilateral renal irradiation with two beams of X-rays targeting both kidneys was performed to deliver a dose of 8.5 Gy. *A*, *right*: unilateral renal irradiation with three beams of X-rays targeting the left kidney was performed to deliver a dose of 8.5 Gy. *B*: serum levels of blood urea nitrogen (BUN) and creatinine (SCr) in preirradiated mice ($n = 6$, bilateral renal irradiation performed 28 days before surgery) and nonirradiated mice ($n = 5$) measured after renal ischemia (for 30 min) and reperfusion (for 48 h) [ischemia-reperfusion (I/R)]. An unpaired parametric test was used to assess statistical significance. *C*, *left*: immunohistochemistry on kidneys of preirradiated and nonirradiated mice following I/R (magnification: ×40) for cell proliferation [proliferating cell nuclear antigen (PCNA)], infiltration of inflammatory cells (CD11b), and total macrophage population (F4/80). *C*, *right*: quantification of positive cells (arrowheads) in the corticomedullary junction in tubular (PCNA) and interstitial (CD11b and F4/80) compartments. An unpaired parametric *t* test was used to assess statistical significance. Data are presented as means ± SD. Significant differences are indicated: $*P < 0.05$, $**P < 0.01$, and $***P < 0.001$ vs. the wild-type control group. Scale bar = 50 μm. *D*, *left*: periodic acid–Schiff (PAS)-stained kidney sections following I/R (magnification: ×40). The ischemic damage was characterized by cell desquamation in nonirradiated kidneys, whereas normal architecture of tubules and cells was observed in preirradiated kidneys. *D*, *right*: histological damage was graded following the Jablonski score. Individual scores are shown as medians and interquartile ranges. A χ^2 test was used to assess statistical significance. Scale bar = 50 μm.

Transcriptomics Analysis (RNA Sequencing)

Powders of kidneys were prepared with biological replicates from the following three experimental groups: "left kidneys of left-irradiated mice" for the kidneys that were directly irradiated (n = 11; irradiated group), "right kidneys of left-irradiated mice" for the kidneys that were directly irradiated (n = 11; contralateral nonirradiated group), and "right kidneys of nonirradiated mice" for kidneys from the mice that were irradiated at all (n = 5; untreated group). Total RNAs were extracted to perform comparative high-throughput RNA sequencing (RNA-Seq).

Sequencing.

Samples were sequenced by the GIGA Genomic Platform on the NextSeq Illumina system. The sequencing was performed using the single-end method with reads of 75 bp.

Data processing and downstream analysis.

FASTQ files are generated from BCL files using "bcl2fastq," and a quality control of the sequences is directly performed using "FastQC" before going further. FASTQ files are then processed for eliminating rRNA and tRNA mapping reads. The reads were then mapped on the Illumina iGenomes hg19 reference using STAR software, and the counts matrix was generated. A quality control of the alignment is performed. Clustering, principal component analysis, and differential expression analysis of the samples were performed using the *R* package "DESeq2" (pairwise comparison between the different experimental conditions). We used DESeq2's median of ratios as the method for normalization, which implies that counts are divided by sample-specific size factors determined by the median ratio of gene counts relative to the geometric mean per gene. This allows gene count comparisons between samples/conditions for differential expression analysis. Differential expression genes are defined using DESeq2 model involving negative binomial (GLM) regression, Wald test, and false discovery rate correction for multiple testing. Functional enrichment analysis was performed using the Database for Annotation, Visualization, and Integrated Discovery (DAVID program).

Real-Time Semiquantitative PCR

Fifty micrograms of kidney powder were homogenized in 1 mL NucleoZOL solution (Macherey-Nagel) supplemented with 400 μL of RNase-free water and incubated at room temperature for 10 min. Lysates were centrifuged at 12,000 *g* at 4°C for 15 min. One milliliter of the supernatant was transferred to a fresh RNase-free tube, and 1 mL of isopropanol (100%) was added to precipitate RNA. The mixtures were centrifuged at 12,000 *g* at 4°C for 10 min, and RNA pellets were washed two times with 500 μL of 75% ethanol before centrifugation at 6,000 *g* at 4°C for 3 min. Pellets were finally dissolved in 100 μL of RNase-free water. RNA concentration and purity were assessed using a NanoDrop Lite spectrophotometer (Thermo Scientific). All RNA samples had an absorbance (260 nm/280 nm) ratio comprised between 1.8 and 2.2. Afterward, cDNAs were generated using a Reverse Transcription Kit (Promega) according to the manufacturer's instructions. Primers used for quantitative RT-PCR are shown in Table 1. Semiquantitative mRNA expression levels were calculated using threshold cycle (C_t) values following the classical $2^{-\Delta Ct}$ equation. The housekeeping gene used for quantitative RT-PCR was *Gapdh*.

^{1}H-NMR Metabolomics Sample Preparation

All samples were recorded at 298 K on a Bruker Avance HD spectrometer operating at 700.17 MHz for the proton signal acquisition. The instrument was equipped with a TCI 5-mm cryoprobe with a *Z*-gradient. Maleic acid was used as the internal standard for quantification and trimethylsilyl-3-propionic acid-d4 (TMSP) for the zero

Table 1. *Primers used for quantitative PCR*

Gene	Direction	Primer Sequence (5′-3′)	Size of the PCR Product, bp	GenBank Accession Number
HO1	Forward	CACTCTGGAGATGACACCTGAG	115	NM_010442
	Reverse	GTGTTCCTCTGTCAGCATCACC		
PECAM1	Forward	CCAAAGCCAGTAGCATCATGGTC	155	NM_008816
	Reverse	GGATGGTGAAGTTGGCTACAGG		
CuZn-SOD	Forward	GGTGAACCAGTTGTGTTGTCAGG	114	NM_011434
	Reverse	ATGAGGTCCTGCACTGGTACAG		
Mn-SOD	Forward	TAACGCGCAGATCATGCAGCTG	133	NM_013671
	Reverse	AGGCTGAAGAGCGACCTGAGTT		
GAPDH	Forward	AAGGTCATCCCAGAGCTGAA	138	NM_008084
	Reverse	CTGCTTCACCACCTTCTTGA		
NOX2	Forward	TGGCGATCTCAGCAAAAGGTGG	150	NM_007807
	Reverse	GTACTGTCCCACCTCCATCTTG		
NOX4	Forward	CGGGATTTGCTACTGCCTCCAT	160	NM_015760
	Reverse	GTGACTCCTCAAATGGGCTTCC		
ALK5	Forward	CTGCCATAACCGCACTGTCA	186	NM_009370
	Reverse	AAATGAAAGGGCGATCTAGTGATG		
HSP70	Forward	ACAAGTCGGAGAACGTGCAGGA	160	NM_010479
	Reverse	GTTGTCCGAGTAGGTGGTGAAG		
HSP27	Forward	GCTCACAGTGAAGACCAAGGAAG	150	NM_013560
	Reverse	TGAAGCACCGAGAGATGTAGCC		
VEGF	Forward	GTCCTGTGTGCCGCTGAT	97	NM_001025250
	Reverse	AGGTTTGATCCGCATGATCT		

ALK5, activin receptor-like kinase 5; CuZn-SOD, superoxide dismutase; HO1, heme oxygenase-1; HSP27, heat shock protein 27; HSP70, heat shock protein 70; Mn-SOD, manganese superoxide dismutase; NOX2, NADPH oxidase; NOX4, NADPH oxidase 4; PECAM1, platelet endothelial cell adhesion molecule-1; VEGF, vascular endothelial growth factor.

calibration. Powders of the kidneys were suspended in 500 μL of deuterated phosphate buffer (pH 7.4), placed on an ice bath, and then subjected to sonication with a vibrating probe (Vibra-Cell, Sonics and Materials) for two periods of 20 s. The mixture was centrifuged (13,300 rotations/min) at 4°C for 10 min to partially eliminate membranes and cell residues. Then, 500 μL of the supernatant were centrifuged a second time through an AMICON ultra 0.5-mL 10-kDa filter tube (13,300 rotations/min, 4°C for 1 h). An aliquot of the filtered sample was withdrawn and added to an adjusted volume of deuterated buffer in a way to keep constant the amount of kidney lysate (±154 mg) in a volume of 300 μL. The adjusted volume was supplemented with 50 μL of a 5 mM solution of maleic acid and 2 μL of a 5 mg/mL TMSP D_2O solution. Samples were lyophilized for 24 h and supplemented with 300 μL of deuterated buffer. ^{1}H-NMR spectra were acquired using a 1-D NOESY sequence with presaturation. The Noesypresat experiment used an RD-90°-T1-90°-Tm-90°-acquire sequence with a relaxation delay of 4 s, a mixing time of 10 ms, and a fixed T1 delay of 4 μs. Water suppression pulse was placed during the relaxation delay. The number of transients was 128 (64 k data points). Data were processed with Bruker Topspin 4.0.8 software with a standard parameter set. Phase and baseline corrections were performed manually over the entire range of the spectra, and the δ-scale was calibrated to 0 ppm using the internal standard TMSP. For statistical analysis, optimized ^{1}H-NMR spectra were automatically baseline-corrected and processed using MestReNova software (version 14.1.1, Mestrelab Research SL). The spectral intensities were normalized to the maleic acid peak and reduced to integrated regions of equal width (0.02 ppm) corresponding to the 0.5- to 9.00-ppm region. Because of the residual signals of water and maleic acid, regions between 4.7 and 5 ppm (water signal) and between 5.6 and 6.2 ppm (maleic acid signal) were removed before analysis. The reduced and normalized NMR spectral data were imported into SIMCA (version 16, Umetrics, Umea Sweden). Multivariate analysis [principal component analysis-X and orthogonal partial least squares discriminant analysis (OPLS-DA)] models of stool metabolomes were used to identify outliers and separation between the groups, respectively. The quality of OPLS-DA models was determined by the predictability calculated on the basis of the fraction correctly predicted in one-seventh cross validation (Q^2); the more this value is near to 1, the better is the model's predictive accuracy. From the OPLS-DA discriminant model, a list of variable importance of projection was generated. Variable importance of projection scores larger than 1 indicate "important" *X*-variables for the discrimination in classes. Metabolite identification was next performed using the open-access database NMR suite 9.0 (Chenomx), the free web-based tool HMDB (http://www.hmdb.ca), and tables. Each metabolite identified was finally confirmed by performing peak correlation plots from 2-D NMR spectra (COSY and HSQC). For univariate analysis of kidney lysates, a one-way ANOVA Kruskal–Wallis test was used for multiple comparisons, whereas Mann–Whitney tests were used for comparisons between two groups.

Histology and Immunostaining

Kidney tissues were fixed in paraformaldehyde for 24 h and then embedded in paraffin. Kidney sections (5 μm) were dewaxed and gradually hydrated before hematoxylin and eosin and periodic acid-Schiff staining. I/R-induced acute tubular necrosis was blindly scored following the Jablonski score. For immunohistochemistry, sections were subjected to antigen retrieval in sodium citrate buffer (pH 6.0, No. S2031, Dako) or target buffer (No. S1699, Dako) or EDTA buffer (No. S2367, Dako). Endogenous peroxidase activity was blocked with 3% hydrogen peroxide (30%, No. 107209, Merck) for 20 min at room temperature. Nonspecific binding was constrained by incubation for 30 min with either normal goat serum or for 10 min with protein block reagent (No. X0909, Dako). Sections were then incubated for 60 min at room temperature with the following primary antibodies: monoclonal mouse antiproliferating cell nuclear antigen (PCNA; No. M0879, Dako, 1/2,500), anti-F4/80 (No. 74383, Abcam, 1/1,000), anti-CD11b (No. 7546 Abcam, 1/6,000), and anti-CD31 antibodies (No. 28364, Abcam, 1/200). After being washed, sections were incubated for 30 min with goat anti-mouse or rabbit biotin-conjugated secondary antibodies (Envision anti-Rabbit/HRP, No. K4003, Dako, 1/400), washed, and exposed to horseradish peroxidase-conjugated streptavidin (1/500) for 30 min. Immunoreactivity was detected using DAB (No. K3468, Dako) or AEC (No. K3464, Dako). Immunohistochemistry scoring was achieved blindly: four randomly selected fields of the corticomedullary region (magnification: ×20) were considered per kidney. Staining was reported to the global number of cells in the considered region (i.e., per cells/mm^2). CD31 immunostaining was quantified blindly on digital images (NanoZoomer 2.0 HT, Hamamatsu). Using the particle plugin for vascular density on the Fiji program (version 1.52i, Wayne Rasban, National Institutes of Health), the images were processed by color deconvolution using a set of macros. The color deconvolution separates the image to isolate the signal from the histological dyes (DAB staining signal), which marks the vessels. A constant threshold was used to exclude the background for all images. The percent area obtained was defined as a percentage of the area of CD31-positive vessels (white pixels) to the total area of the slice. The following formula was used to calculate vascular density: vascular density = vessel area/total area × 100%.

Drug Preparation and Administration

Sunitinib malate/SU11248/SUTENT was purchased from LC Laboratories (Woburn, MA). Sunitinib (4 mg/mL) was suspended in vehicle consisting of 0.5% carboxymethylcellulose, 1.8% NaCl, 0.4% Tween 80, 0.9% benzyl alcohol, and ultrapure water adjusted to pH 6.0. Drug aliquots were stored in the dark at −20°C. Animals were administered daily by oral gavage with vehicle or sunitinib (40 mg/kg/day) for 14 days before I/R.

Statistical Analyses

Data are expressed as means ± SD. Data normality was measured using four normality tests (D'Agostino-Pearson, Anderson–Darling, Shapiro–Wilk, and Kolmogorov–Smirnov). An unpaired-parametric *t* test or ordinary one-way ANOVA (Tukey's multiple-comparisons test) were used in case the normality test was passed, and an unpaired nonparametric

test (Mann–Whitney) or Kruskal–Wallis test (Dunn's multiple-comparisons test) were used in case the normality test was not passed. A χ^2-test was used to compare discrete variables with a P value of ≤ 0.05 considered as the statistically significant threshold. Analysis of data was performed using GraphPad PRISM software (GraphPad Software, La Jolla, CA).

RESULTS

Kidney-Centered Irradiation Attenuates Renal I/R Injury at 28 Days Postirradiation

Renal ischemic injury is classically associated with an increased accumulation of AKI biomarkers in blood, including

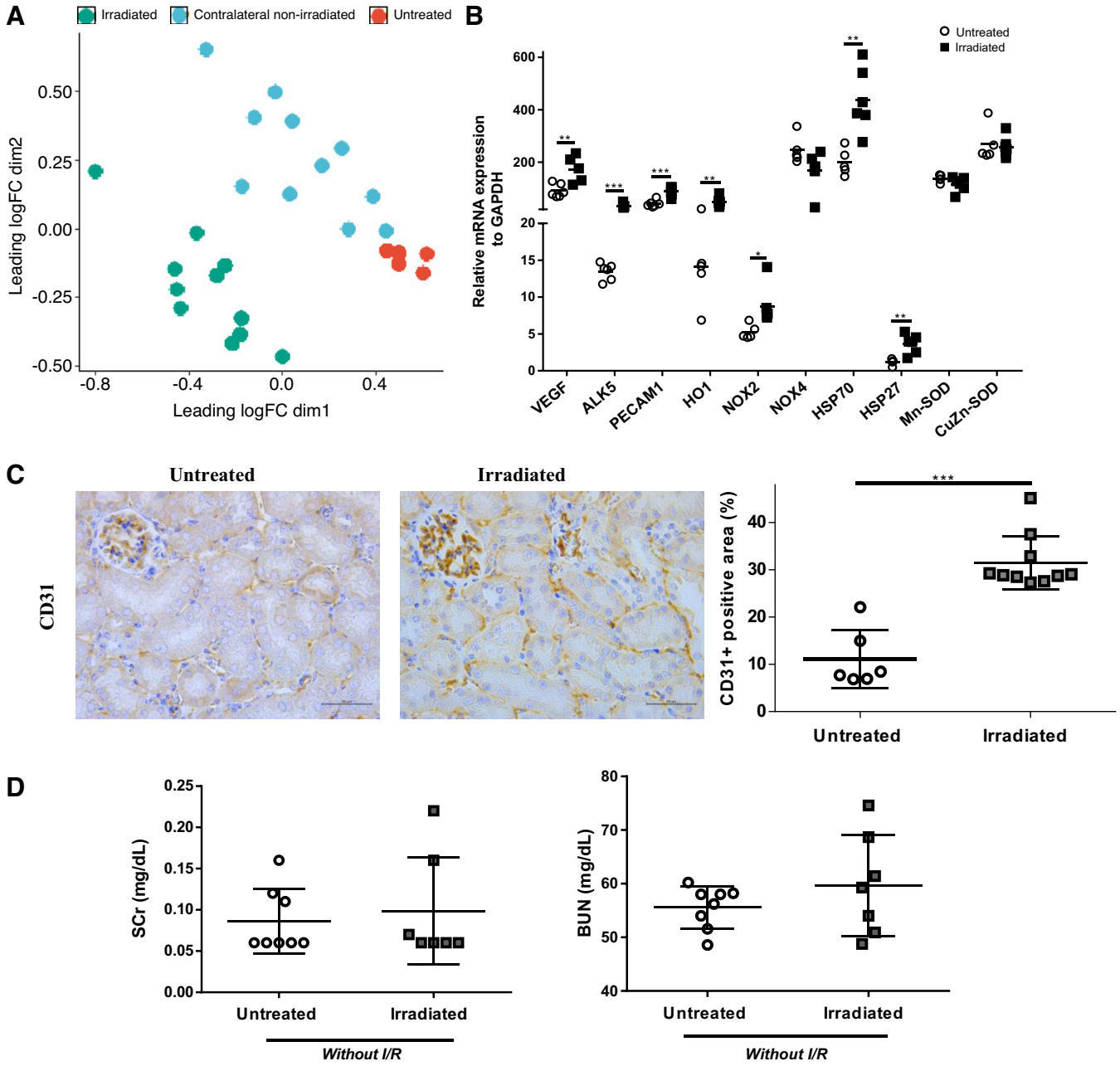

Figure 2. *A*: dimensionality reduction of RNA-sequencing analysis, in which the following three groups are shown: "left kidneys of left-irradiated mice" for the kidneys that were directly irradiated (n = 11; irradiated group), "right kidneys of left-irradiated mice" for the kidneys that were not directly irradiated (n = 11; contralateral nonirradiated group), and "right kidneys of nonirradiated mice" for kidneys from mice that were not irradiated at all (n = 5; untreated group). *B*: quantitative real-time PCR quantification of mRNA expression levels of vascular endothelial growth factor (*VEGF*), transforming growth factor-β receptor I [activin receptor-like kinase 5 (*ALK5*)], platelet endothelial cell adhesion molecule-1 (*PECAM1* or CD31), heme oxygenase-1 (*HO1*), cytochrome *b*-245 [NADPH oxidase 2 (*NOX2*)], NADPH oxidase 4 (*NOX4*), heat shock protein 70 (*HSP70*), heat shock protein 27 (*HSP27*), manganese superoxide dismutase (*Mn-SOD*), and superoxide dismutase (*CuZn-SOD*). *C*: cross sections of kidneys labeled for CD31-positive vascular density in irradiated and untreated groups (magnification: x40). Irradiated mice showed higher renal vascular density. An unpaired parametric test was used to assess statistical significance. $^*P < 0.05$, $^{**}P < 0.01$, and $^{***}P < 0.001$. *D*: biological analyses at *day 28* after bilateral renal irradiation without renal I/R. Serum levels of blood urea nitrogen (BUN) and creatinine (SCr) in irradiated (n = 7) and untreated mice (n = 8) are shown. Data are presented as means ± SD. FC, fold change; I/R, ischemia-reperfusion.

Table 2. *Upregulated signaling pathways mostly impacted by irradiation per se (i.e., in the left kidneys) after subtraction of the influence of remote exposure of the contralateral right kidneys: cross analysis between "irradiated kidneys vs. untreated kidneys" against "contralateral nonirradiated kidneys vs. untreated kidneys"*

Upregulation	*P* Value	Genes	Fold Enrichment
Regulation of angiogenesis	0.002	*ALK5, HMOX1, TGFBI, ITGB1, XBP1, ITGB3, SPHK1, SERPINE1, STAT3, ITGB2, GAB1, PIK3CD, HSPB1, SIRT1, RHOB, STIM1, PTK2B, PRKD2*	2.8
Regulation of cell cycle	0.003	*CDKN1A, HSP90AB1, PTEN, FBXL22, RASSF1, MYC, EPC1, SFN, SKIL, CLIC1, HSPA8, JUN, NPM1, STAT3, OVOL2, GADD45G, BOP1, SFPQ, RGCC, MORF4L2, DDIT3, GAS2, SGK1, BIRC2*	2.2
Regulation of cell proliferation	0.03	*YAP1, ITGB1, CSF1R, PTEN, YBX1, EGFR, PLAC8, EDNRB, MYC, PDGFD, GCNT2, S1PR1, PTK2B, AKIRIN2, JUN, XBP1, NPM1, TGFB3, SPHK1, F2R, STAT3, CCDC117, OSMR, SIRT1, ACER2, FABP4, CLDN7, KIF20B, SLC25A33, CACUL1, ATF3, BCL2L1, HBEGF*	2.3
Vascular endothelial growth factor signaling pathway	0.01	*XBP1, SPHK1, GAB1, HSPB1, PRKD2, NUS1, PIK3CA, C5AR1, EIF2AK3, ATF4, C3, SULF2, XBP1, VCAM1, HSPB1, PRKD2XBP1, VCAM1, HSPB1, PRKD2*	6.2
Stress response	0.001	*HSPA1B, HSPA1A, PPP1R15A, HSPA8, XBP1, HSP90AA1, HSP90AB1, HSPB8, HSPA4L, AHSA2, EIF2AK3, AHSA1, HSPB1, HSPE1, MANF, DNAJB1, HSPH1, DDIT3, CHORDC1, SERPINH1*	6.1
Cellular response to transforming growth factor-β stimulus	0.008	*ALK5, CREB1, TGFB3, STAT3, ZYX, GCNT2, JUN, MTMR4, SKIL, SIRT1, FERMT2, ATF3, APAF1, EGFR*	3.1
Cellular response to hypoxia	0.002	*NPM1, PTEN, STC1, AK4, MIEF1, CFLAR, FOXO3, SIRT1, VASN, ZFP36L1, BBC3, RGCC, CR1L, MYC, ANKRD1, UBQLN1, PCK1*	3.8

SCr and BUN, and with inflammation of the renal parenchyma assessed by cell proliferation (PCNA) and infiltration of inflammatory cells (CD11b and F4/80). One month after kidney-centered bilateral irradiation (Fig. 1*A*), SCr and BUN levels were significantly lower in preirradiated compared with untreated animals following I/R (SCr: 0.5 ± 0.2 vs. 2.4 ± 0.4 mg/dL and BUN: 148.4 ± 41.6 vs. 495.7 ± 13.5 mg/dL, $P < 0.01$; Fig. 1*B*). The renal infiltration by CD11b-positive cells (187 ± 32 vs. 477 ± 20/mm^2) and F4/80 macrophages (110 ± 22 vs. 212 ± 25/mm^2) as well as the number of proliferating PCNA-positive cells (131 ± 53 vs. 545 ± 257 cells/mm^2) were significantly reduced in preirradiated kidneys ($P < 0.001$; Fig. 1*C*). Furthermore, the Jablonski score of acute tubular necrosis on periodic acid-Schiff-stained kidney sections was significantly lower in the irradiated group ($P < 0.01$; Fig. 1*D*). Of important note, no difference was observed between sham-operated preirradiated and untreated animals in the AKI biomarkers SCr and BUN (Fig. 2*D*). Altogether, these data suggest that kidney-centered irradiation 28 days before I/R induces IPC and promotes resistance against I/R injury, with preserved functional and structural properties of the kidney.

Comparative Transcriptomics Reveals a Significant Upregulation of Signaling Pathways Involved in Angiogenesis and the Stress Response Following Kidney-Centered Irradiation

To decipher the mechanisms by which renal irradiation establishes the observed IPC, we performed unilateral renal irradiation without I/R (Fig. 1*A*). Total RNAs were extracted to

Table 3. *Downregulated signaling pathways mostly impacted by irradiation per se (i.e., in the left kidneys) after subtraction of the influence of remote exposure of the contralateral right kidneys: cross analysis between "irradiated kidneys vs. untreated kidneys" against "contralateral nonirradiated kidneys vs. untreated kidneys"*

Downregulation	*P* Value	Genes	Fold Enrichment
Oxidoreductase activity	0.03	*FADS6, SCD2, FADS1, PECR, MIOX, HSD3B2, GPX3, ACADSB, CYP2D26, NOX4, CHDH, GPD1, PYROXD2, ALDH5A1*	9.4
Glutathione metabolic process	0.03	*GSTM1, GSTO2, TXNRD3, ETHE1, IDH1, GSTA2, GSR, CBR1, GSTM1, GSTO2, GSTA2, PTGES*	2.8
Regulation of JNK cascade	0.03	*MAPK9, MAP3K1, MAP3K7, TLR3, MAP3K12, ZEB2, VANGL2, MAP3K1, FZD8, MAP3K7, MAP3K12, EDAR, GADD45A, DIXDC1, DUSP15, MAPK8IP1*	3.4
Regulation of catalytic activity	0.02	*APOBEC1, ALAS2, RSAD2, MOCOS, GMPR, NMNAT3, SLC3A2, KLHL3, ACCS, ACACB, KYNU, PGGT1B, ALPL, HACL1, CKB, MOCS1, CAMK1G, BCAT2, FDFT1, PCGF2, PRKAG2, ELMOD3, GPT2*	1.5
Positive regulation of cell migration	0.02	*PDGFRB, SEMA6C, SEMA4A, ABCC1, SYNPO2, SEMA6D, SEMA3B, LAMB1, IGF1, ETS1, CXCL12, PODXL, PLP1, KDR, ITGA6*	1.7
Positive regulation of vasoconstriction	0.003	*TBXA2R, GJA5, AVPR2, PTGER3, TBXAS1, ABL1, SMTNL2, SMAD6, ADRA1A*	4.9

A

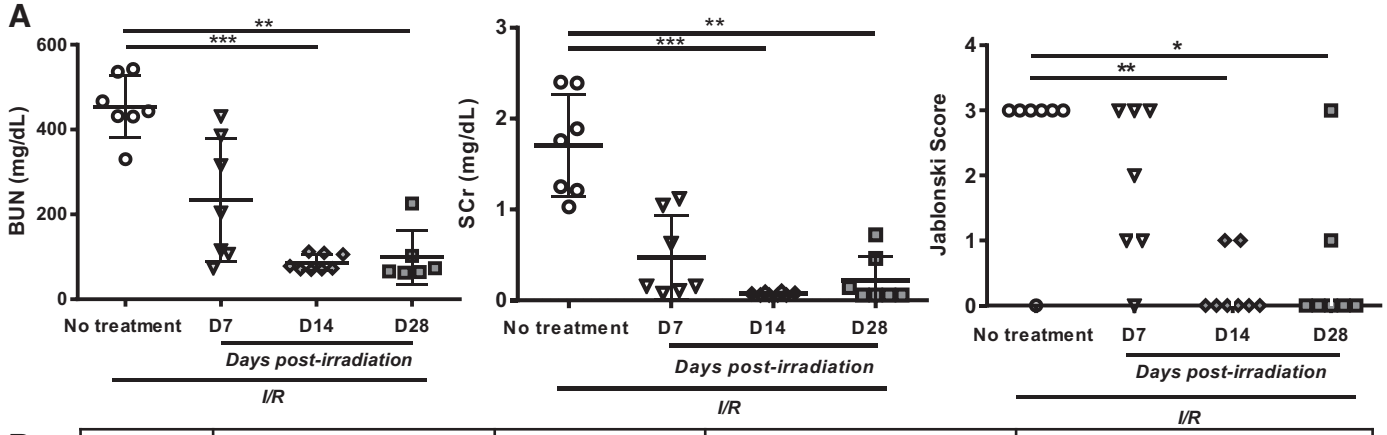

B

IHC/Fiji	*Renal inflammation post-I/R*	*No treatment*	*D7 post-irradiation*	*D14 post-irradiation*
Positive Cells/mm²	PCNA-positive cells	563.0± 38.62 *	242.4± 69.16	111.9± 36.04 *
	CD11b-positive cells	502.7± 34.01*	262.2± 62.99	203.2± 31.10*
	F4/80-positive cells	269.7± 18.32 *	201.3± 28.74	138,0± 23.27 *

C

RTqPCR	*Angiogenesis and stress response markers*	*No treatment*	*D7 post-irradiation*	*D14 post-irradiation*
Relative mRNA expression to GAPDH	VEGF	0.024± 0.004 *$	0.041± 0.004 *	0.057± 0.007 *$
	ALK5	0.007± 0.001 *$	0.010± 0.001 *	0.037± 0.005 *$
	PECAM1	0.006± 0.002 *$	0.012± 0.002 *	0.070± 0.013 *$
	HO1	0.005± 0.001 *	0.007± 0.002	0.016± 0.002 *
	HSP70	0.072± 0.020	0.081± 0.007	0.101± 0.037
	HSP27	0.001± 0.0008	0.001± 0.0007	0.001± 0.0007

D

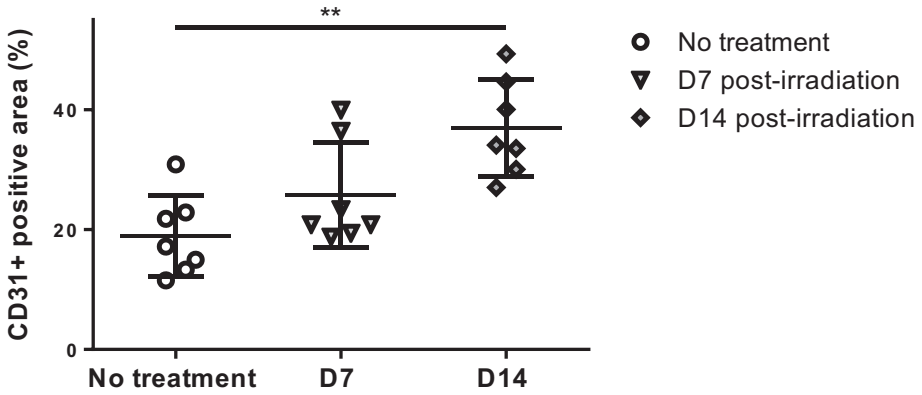

Figure 3. *A*: renal function and damage assessed by serum creatinine (SCr), blood urea nitrogen (BUN), and Jablonski score after 48-h postischemia-reperfusion (I/R) in untreated mice and irradiated mice 7, 14, and 28 days after bilateral renal irradiation (n = 7/group). Renal function was significantly protected after 14 days postirradiation. *B*: quantification of cell proliferation [proliferating cell nuclear antigen (PCNA)], infiltration of inflammatory cells (CD11b), and total macrophage population (F4/80) on I/R kidneys of untreated and irradiated mice 7 days (D7) and 14 days (D14) postirradiation. Values are represented as means ± SE. *$P < 0.05$ by one-way ANOVA. *C*: quantitative real-time PCR (RTqPCR) quantification of mRNA expression levels of vascular endothelial growth factor (*VEGF*), transforming growth factor-β receptor I [activin receptor-like kinase 5 (*ALK5*)], platelet endothelial cell adhesion molecule-1 (*PECAM1* or CD31), heme oxygenase-1 (*HO1*), heat shock protein 70 (*HSP70*), and heat shock protein 27 (*HSP27*) in kidneys from untreated and irradiated mice 7 and 14 days postirradiation. Values are represented as means ± SE. *$$P < 0.05$ by one-way ANOVA. *D*: renal vascular density assessed by the CD31-positive network in untreated mice and irradiated mice 7 and 14 days postirradiation. Renal vascularization significantly increased 14 days postirradiation. One-way ANOVA (Kruskal–Wallis test) was used to assess statistical significance. *$P < 0.05$, **$P < 0.01$, and ***$P < 0.001$. IHC, immunohistochemistry.

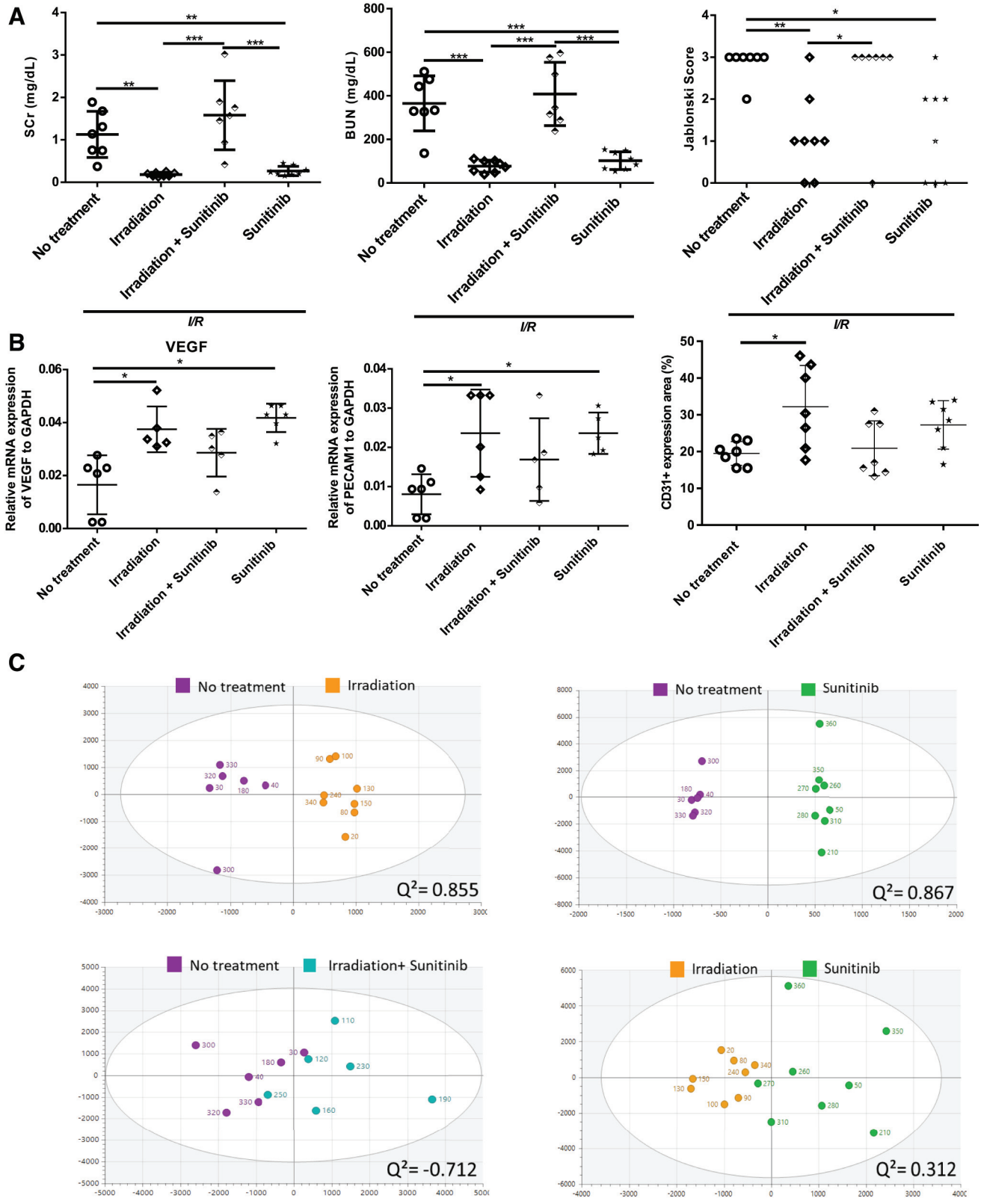

perform comparative high-throughput RNA-Seq between the following three experimental groups: irradiated (n = 11), contralateral nonirradiated (n = 11), and untreated (n = 5). Among 24,411 genes, 1,818 genes were found to be differentially expressed 28 days following irradiation. We further applied multidimensional scaling to order samples in a two-dimensional scatterplot. The three groups of mice did not overlap, meaning a distinct transcriptomics pattern, specific to each

group (Fig. 2*A*). Renal irradiation was significantly associated with the upregulation of signaling pathways involved in angiogenesis, cell proliferation, and the stress response and downregulation of oxidoreduction (Tables 2 and 3).

Real-time quantitative RT-PCR was used to further characterize the identified pathways. Markers of angiogenesis [vascular endothelial growth factor (*VEGF*), activin receptor-like kinase 5 (*ALK5*), heme oxygenase-1 (*HO1*), and platelet endothelial cell adhesion molecule-1 (*PECAM1*)] and the stress response [heat shock protein 70 (*HSP70*), heat shock protein 27 (*HSP27*), and NADPH oxidase 2 (*NOX2*)] were highlighted with a significant increase in the irradiated group compared with the untreated group ($P < 0.01$; Fig. 2*B*). Following these observations, we evaluated the renal vascular network. Nonischemic irradiated kidneys were characterized by an increased surface of the CD31-positive vascular area compared with untreated kidneys (11.2 ± 2.5 vs. 31.5 ± 1.8, $P < 0.001$; Fig. 2*C*).

Renal Protection and Vascularization Are Significantly Induced 14 Days Postirradiation

Our data suggest that 8.5-Gy irradiation focused on the kidneys is associated with *1*) renal IPC against an episode of I/R occurring 1-mo postirradiation (Fig. 1) as well as *2*) an increase in renal vascularization (Fig. 2, *B* and *C*). To determine the shortest efficient delay to induce renal IPC, renal I/R was performed at 7, 14, and 28 days after bilateral renal irradiation. Following I/R, BUN and SCr levels as well as renal damage were significantly lower in irradiated mice compared with untreated mice starting from *day 14* postirradiation (Fig. 3*A*). Similarly, renal inflammation after I/R was significantly attenuated at *day 14* postirradiation (Fig. 3*B*). No significant renal IPC was observed at *day 7* postirradiation. Nonischemic irradiated kidneys were characterized by increased expression of the vascular markers *ALK5*, *VEGF*, and *PECAM1* at the mRNA level compared with untreated kidneys, as early as *day 7* postirradiation (Fig. 3*C*). The CD31-positive vascular area was significantly increased from *day 14* following irradiation (Fig. 3*D*). Taken together, these observations suggest that renal irradiation promotes renal angiogenesis within 14 days postirradiation, which may participate in the observed IPC.

Irradiation-Induced Renal Protection Is Blunted by the Antiangiogenic Drug Sunitinib

Angiogenesis may be implicated in irradiation-induced renal IPC. We used a classical pharmacological approach based on sunitinib malate, a multitargeted inhibitor of VEGFreceptors, platelet-derived growth factor receptors, and other coactivators of angiogenesis, to block neoangiogenesis, and tested the impact of irradiation on renal IPC under such conditions (21). The following four groups were compared: mice irradiated (8.5 Gy on both kidneys) and treated with sunitinib (*group 1*), mice irradiated (8.5 Gy on both kidneys) and treated with vehicle (*group 2*), control mice not irradiated and treated with sunitinib (*group 3*), and control mice not irradiated and treated with vehicle (*group 4*).

One-way ANOVA followed by Tukey's test showed that, following I/R, serum levels of SCr and BUN were significantly lower in irradiated compared with *1*) untreated mice (BUN: 106.1 ± 33.6 vs. 352.2 ± 54.3 mg/dL and SCr: 0.3 ± 0.13 vs. 1 ± 0.2 mg/dL) and *2*) irradiated mice treated with sunitinib (BUN: 106.1 ± 33.6 vs. 408.4 ± 54.9 mg/dL and SCr: 0.3 ± 0.12 vs. 1.5 ± 0.3 mg/dL; Fig. 4*A*). No difference was observed between irradiated mice treated with sunitinib and untreated mice. Jablonski severity score was lower in the irradiated group compared with the irradiated group treated with sunitinib and the untreated group ($P < 0.01$; Fig. 4*A*). Of note, the group treated with sunitinib also showed a nephroprotective profile compared with the untreated group. At the mRNA level, renal expression of *VEGF* and *PECAM1* was increased in the irradiated group and sunitinib-treated group ($P < 0.01$). At the histological level, the CD31-positive vascular area was significantly increased only in the renal parenchyma of the irradiated group (Fig. 4*B*).

NMR-Based Metabolomics Reveals Distinct Metabolic Patterns of Renal IPC Following Renal Irradiation or Exposure to Sunitinib Malate

OPLS-DA applied to the ^{1}H-NMR spectra data of the four abovementioned experimental groups showed a significant discrimination between untreated versus both irradiated and nonirradiated sunitinib-treated kidneys (Fig. 4*C*). The previously identified (22) metabolomics signature of renal I/R was found in both untreated and irradiated sunitinib-treated groups, with increased levels of creatine, lactate, and isoleucine and decreased levels of choline, taurine, and myo-inositol. In contrast, this metabolomics signature was attenuated in irradiated and nonirradiated sunitinib-treated groups (Fig. 5*A*). More importantly, comparative metabolomics both at baseline (Fig. 5*B*) and after I/R between irradiated and nonirradiated sunitinib-treated groups did not overlap, indicating distinct metabolic patterns of renal IPC in each group.

DISCUSSION

The management of AKI remains complex, and a better understanding of the pathophysiology of AKI may help to find innovative pharmacological targets and cell-based therapies (6, 23), or lipotoxicity attenuation (8, 24). Our present study investigated the impact of kidney irradiation on kidney function, structure, and vascularization following I/R

Figure 4. *A*: renal functional and structural damage assessed by serum creatinine (SCr), blood urea nitrogen (BUN), and Jablonski score after 48 h post-ischemia-reperfusion (I/R) in untreated mice, irradiated mice treated with vehicle, irradiated mice treated with sunitinib malate, and mice only treated with sunitinib malate ($n = 8$). *B*: quantitative real-time PCR quantification of mRNA expression levels of vascular endothelial growth factor (*VEGF*) and platelet endothelial cell adhesion molecule-1 (*PECAM1*) and renal vascularization assessed by the CD31-positive network. One-way ANOVA (Tukey's test) was used to assess statistical significance. $*P < 0.05$, $**P < 0.01$, and $***P < 0.001$. *C*: score plot from orthogonal partial least squares discriminant analysis (OPLS-DA) applied to ^{1}H-NMR spectra of kidney lysates following renal I/R and corresponding treatment (on the axes the principal components explaining the variance). *C*, *top left*: OPLS-DA for no treatment vs. irradiation groups (n comp = 3, $R^2 = 0.842$, $Q^2 = 0.855$). *C*, *top right*: OPLS-DA for no treatment vs. sunitinib groups (n comp = 8, $R^2 = 0.982$, $Q^2 = 0.867$). *C*, *bottom left*: OPLS-DA for no treatment vs. irradiation + sunitinib-treated groups (n comp = 2, $R^2 = 0.723$, $Q^2 = -0.712$. *C*, *bottom right*: OPLS-DA for irradiation vs. sunitinib-treated groups (n comp = 2, $R^2 = 0.886$, $Q^2 = 0.312$).

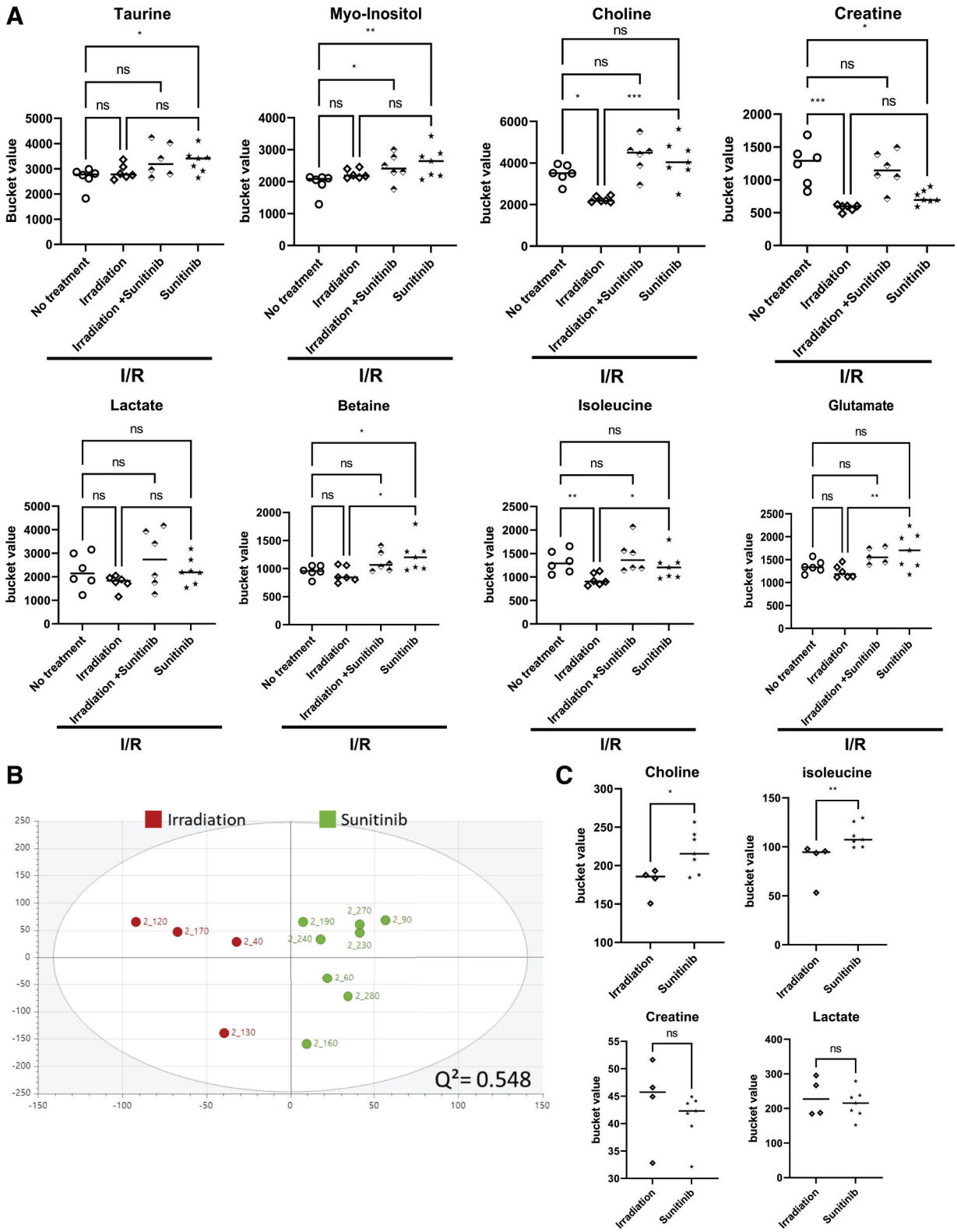

Figure 5. *A*: univariate analysis for the most relevant metabolites of kidney lysates following renal ischemia-reperfusion (I/R) and the corresponding treatment (*$P < 0.05$, **$P < 0.01$, and ***$P < 0.001$). *B*: score plot from orthogonal partial least squares discriminant analysis (OPLS-DA) applied to ^{1}H-NMR spectra of kidney lysates following irradiation or treatment with sunitinib malate (n comp = 3, $R^2 = 0.831$, $Q^2 = 0.548$) (on the axes the principal components explaining the variance). *C*: univariate analysis for several relevant metabolites of kidney lysates following irradiation or treatment with sunitinib malate (*$P < 0.05$, **$P < 0.01$, and ***$P < 0.001$). ns, not significant.

in mice. We used the SmART microirradiator device, which has been shown to be effective in the precise targeting of a specific organ in small animals including rodents (20, 25). We observed that kidney-centered irradiation performed at least 14 days before the ischemic insult was nephroprotective against I/R, with reduced serum levels of SCr and BUN in irradiated mice after 30 min of ischemia and 48 h of reperfusion. This protection was associated with a significant reduction of the 4-grade Jablonski score (based on the extent of proximal tubule necrosis), which has been validated in the assessment of I/R-induced acute tubular necrosis (26, 27). Following I/R, the inflammatory response, as measured by PCNA, CD11b, and F4/80 inflammation markers, was also attenuated in the renal parenchyma in irradiated kidneys. This irradiation-induced renal IPC was associated with the activation of angiogenesis pathways, and it was blunted by the oral administration of the antiangiogenic agent sunitinib. Therapeutic angiogenesis for the treatment of renal disease has been reported in a previous study (28). Several reports have demonstrated that VEGF treatment protects rats from widespread necrosis, glomerular injury, and apoptosis of glomerular and tubulointerstitial cells in rat models of renal thrombotic microangiopathy (29, 30). Engel et al. (30) showed that kidney-specific VEGF therapy in experimental renovascular disease in pigs triggers the recovery of renal function. In a similar mouse model of renal I/R, we have recently demonstrated that dual-specificity phosphatase 3 deletion induces renal IPC associated with increased renal vascular density, increased phosphorylation of peptides involved in VEGF-related angiogenesis, and reduced renal inflammation (31).

In addition to the inflammatory response, the hypoxia that follows I/R may activate angiogenic factors, such as VEGF, and may be beneficial by stabilizing the microvasculature and favoring local blood supplies (32, 33). Previous work has shown that irradiation induces increased vascularization in renal tissue (34–36). Our comparative transcriptomics highlights an upregulation of angiogenesis circuits after kidney-centered irradiation. Furthermore, the CD31-positive vascular network was significantly increased in the renal parenchyma of irradiated mice compared with controls. We noted increased mRNA expression levels of the angiogenesis markers *ALK5*, *VEGF*, *HO1*, and *PECAM1*, which may participate in the renal IPC observed in irradiated mice. To investigate this hypothesis, we used the antiangiogenic drug sunitinib malate to block neovascularization postirradiation, by comparing irradiated mice treated or not with sunitinib malate with controls. Significant IPC was confirmed in irradiated mice, whereas such nephroprotection was blunted in irradiated mice treated with sunitinib malate. Unexpectedly, the group of animals with no irradiation but with exposure to sunitinib malate showed an attenuation of renal I/R injury. Previous studies have pointed to the fact that sunitinib, which is classically used to block tumor neoangiogenesis, could be proangiogenic in normal tissue via the stimulation of VEGF expression (37, 38). Our quantitative RT-PCR analyses compared with control kidneys detected increased expression of VEGF in the irradiated group and in the nonirradiated group treated with sunitinib, with no significant changes in the group that combined irradiation and sunitinib treatment. The extent of the CD31-positive vascular network was only significantly increased in the irradiated group. Of important note, the sunitinib used in our study was in the form of a malate salt. The pharmacological influence of various salts in the IPC process has been previously suggested (39). In particular, malate is an agonist of the succinate receptor (40), which may be potentially involved in IPC (41). In our comparative metabolomics, the renal I/R metabolic signature (22) was attenuated after I/R surgery following irradiation or sunitinib malate treatments. Interestingly enough, the comparative metabolomics at baseline and after I/R between irradiated versus nonirradiated sunitinib-treated groups revealed distinct metabolic patterns. Such a sunitinib malate-mediated nephroprotection against I/R deserve further in-depth characterization.

As a whole, modulating/expanding the renal vasculature may help accelerate the perfusion and oxygenation of the organ following an ischemic insult (4, 33). Renal irradiation leads to expanding vascularization, which potentially plays a role in such an established renal IPC against I/R.

Perspectives and Significance

Our observations indicate that kidney-focused irradiation activates angiogenic pathways in the renal parenchyma and is nephroprotective in case of I/R-induced AKI. The modulation of the molecular targets of irradiation-induced renal IPC may open new avenues in the development of innovative pharmacological strategies against a major medical problem, which is perioperative acute ischemic kidney injury.

ACKNOWLEDGMENTS

The authors acknowledge Christophe Bovy (Division of Nephrology) for scoring the renal acute tubular necrosis as well as Arnaud Lavergne (GIGA Genomics platform) and Laurence Poma (Laboratory of Translational Research in Nephrology), ULiège CHU, for technical assistance.

GRANTS

This work was supported by the Belgian National Fund for Scientific Research and by the University of Liège (Fonds Léon Fredericq and Fonds Spéciaux à la Recherche) (to B.K. and F.J.) and by Swiss National Science Foundation (to S.D.S.).

DISCLOSURES

No conflicts of interest, financial or otherwise, are declared by the authors.

AUTHOR CONTRIBUTIONS

B.K. and F.J. conceived and designed research; B.K., F.L., and P.R. performed experiments; B.K., A.C., P.R., D.L., P.D.T., and F.J. analyzed data; B.K., F.L., P.R., D.L., N.E.S., A.N., S.d.S., and F.J. interpreted results of experiments; B.K. prepared figures; B.K. drafted manuscript; B.K., F.L., A.C., P.R., D.L., N.E.S., A.N., P.D.T., S.d.S., and F.J. edited and revised manuscript; B.K., F.L., A.C., P.R., D.L., N.E.S., A.N., P.D.T., S.d.S., and F.J. approved final version of manuscript.

REFERENCES

1. **Hoste EAJ**, **Kellum JA**, **Selby NM**, **Zarbock A**, **Palevsky PM**, **Bagshaw SM**, **Goldstein SL**, **Cerdá J**, **Chawla LS.** Global

epidemiology and outcomes of acute kidney injury. *Nat Rev Nephrol* 14: 607–625, 2018. doi:10.1038/s41581-018-0052-0.

2. **Ali T**, **Khan I**, **Simpson W**, **Prescott G**, **Townend J**, **Smith W**, **MacLeod A.** Incidence and outcomes in acute kidney injury: a comprehensive population-based study. *J Am Soc Nephrol* 18: 1292–1298, 2007. doi:10.1681/ASN.2006070756.
3. **Singh AP**, **Junemann A**, **Muthuraman A**, **Jaggi AS**, **Singh N**, **Grover K**, **Dhawan R.** Animal models of acute renal failure. *Pharmacol Rep* 64: 31–44, 2012. doi:10.1016/S1734-1140(12)70728-4.
4. **Bonventre JJV**, **Yang L.** Cellular pathophysiology of ischemic acute kidney injury. *J Clin Invest* 121: 4210–4221, 2011. doi:10.1172/JCI45161.
5. **Rowart P**, **Erpicum P**, **Detry O**, **Weekers L**, **Grégoire C**, **Lechanteur C**, **Briquet A**, **Beguin Y**, **Krzesinski J-M**, **Jouret F.** Mesenchymal stromal cell therapy in ischemia/reperfusion injury. *J Immunol Res* 2015: 1–8, 2015. doi:10.1155/2015/602597.
6. **Erpicum P**, **Rowart P**, **Poma L**, **Krzesinski J-M**, **Detry O**, **Jouret F.** Administration of mesenchymal stromal cells before renal ischemia/reperfusion attenuates kidney injury and may modulate renal lipid metabolism in rats. *Sci Rep* 7: 8687, 2017. doi:10.1038/s41598-017-08726-z.
7. **Kalogeris T**, **Baines CP**, **Krenz M**, **Korthuis RJ.** Cell biology of ischemia/reperfusion injury. *Int Rev Cell Mol Biol* 298: 229–317, 2012. doi:10.1016/B978-0-12-394309-5.00006-7.
8. **Erpicum P**, **Rowart P**, **Defraigne J-O**, **Krzesinski J-M**, **Jouret F.** What we need to know about lipid-associated injury in case of renal ischemia-reperfusion. *Am J Physiol Renal Physiol* 315: F1714–F1719, 2018. doi:10.1152/ajprenal.00322.2018.
9. **Legrand M**, **Rossignol P.** Cardiovascular consequences of acute kidney injury. *N Engl J Med* 382: 2238–2247, 2020. doi:10.1056/NEJMra1916393.
10. **Erpicum P**, **Detry O**, **Weekers L**, **Bonvoisin C**, **Lechanteur C**, **Briquet A**, **Beguin Y**, **Krzesinski J-M**, **Jouret F.** Mesenchymal stromal cell therapy in conditions of renal ischaemia/reperfusion. *Nephrol Dial Transplant* 29: 1487–1493, 2014. doi:10.1093/ndt/gft538.
11. **Gameiro J**, **Fonseca JA**, **Outerelo C**, **Lopes JA.** Acute kidney injury: from diagnosis to prevention and treatment strategies. *J Clin Med* 9: 1704, 2020. doi:10.3390/jcm9061704.
12. **Veighey K**, **MacAllister R.** Clinical applications of remote ischaemic preconditioning in native and transplant acute kidney injury. *Pediatr Nephrol* 30: 1749–1759, 2015. doi:10.1007/s00467-014-2965-6.
13. **Tu YP**, **Chen SC**, **Liu YH**, **Chen CF**, **Hour TC.** Postconditioning with far-infrared irradiation increases heme oxygenase-1 expression and protects against ischemia/reperfusion injury in rat testis. *Life Sci* 92: 35–41, 2013. doi:10.1016/j.lfs.2012.10.019.
14. **Lakyová L**, **Toporcer T**, **Tomečková V**, **Sabo J**, **Radonõak J.** Low-level laser therapy for protection against skeletal muscle damage after ischemia-reperfusion injury in rat hindlimbs. *Lasers Surg Med* 42: 665–672, 2010. doi:10.1002/lsm.20967.
15. **Nomura T**, **Li X-H**, **Ogata H**, **Sakai K**, **Kondo T**, **Takano Y**, **Magae J.** Suppressive effects of continuous low-dose-rate γ irradiation on diabetic nephropathy in type II diabetes mellitus model mice. *Radiat Res* 176: 356–365, 2011. doi:10.1667/rr2559.1.
16. **Taylor K**, **Lemon JA**, **Phan N**, **Boreham DR.** Low-dose radiation from 18 F-FDG PET does not increase cancer frequency or shorten latency but reduces kidney disease in cancer-prone *Trp53*+/− mice. *Mutagenesis* 29: 289–294, 2014. doi:10.1093/mutage/geu017.
17. **Kim J**, **Park JW**, **Park KM.** Increased superoxide formation induced by irradiation preconditioning triggers kidney resistance to ischemia-reperfusion injury in mice. *Am J Physiol Renal Physiol* 296: F1202–F1211, 2009. doi:10.1152/ajprenal.90592.2008.
18. **Verhaegen F**, **Granton P**, **Tryggestad E.** Small animal radiotherapy research platforms. *Phys Med Biol* 56: R55–R83, 2011. doi:10.1088/0031-9155/56/12/R01.
19. **Grandinetti J**, **Zhong Y**, **Shen C**, **Jia X.** Design and experimental validation of a unilateral magnet for MRI-guided small animal radiation experiments. *J Magn Reson* 332: 107062, 2021. doi:10.1016/j.jmr.2021.107062.
20. **Clarkson R**, **Lindsay PE**, **Ansell S**, **Wilson G**, **Jelveh S**, **Hill RP**, **Jaffray DA.** Characterization of image quality and image-guidance performance of a preclinical microirradiator. *Med Phys* 38: 845–856, 2011. doi:10.1118/1.3533947.
21. **Christensen JG.** A preclinical review of sunitinib, a multitargeted receptor tyrosine kinase inhibitor with anti-angiogenic and antitumour activities. *Ann Oncol* 18, Suppl 10: x3–x10, 2007. doi:10.1093/annonc/mdm408.
22. **Jouret F**, **Leenders J**, **Poma L**, **Defraigne J-O**, **Krzesinski J-M**, **de Tullio P.** Nuclear magnetic resonance metabolomic profiling of mouse kidney, urine and serum following renal ischemia/reperfusion injury. *PLoS One* 11: e0163021, 2016. doi:10.1371/journal.pone.0163021.
23. **Tögel FE**, **Westenfelder C.** Mesenchymal stem cells: a new therapeutic tool for AKI. *Nat Rev Nephrol* 6: 179–183, 2010. doi:10.1038/nrneph.2009.229.
24. **Kaushal GP**, **Shah SV.** Challenges and advances in the treatment of AKI. *J Am Soc Nephrol* 25: 877–883, 2014. doi:10.1681/ASN.2013070780.
25. **Donis N**, **Jiang Z**, **D'Emal C**, **Hulin A**, **Debuisson M**, **Dulgheru R**, **Nguyen ML**, **Postolache A**, **Lallemand F**, **Coucke P**, **Martinive P**, **Herzog M**, **Pamart D**, **Terrell J**, **Pincemail J**, **Drion P**, **Delvenne P**, **Nchimi A**, **Lancellotti P**, **Oury C.** Differential biological effects of dietary lipids and irradiation on the aorta, aortic valve, and the mitral valve. *Front Cardiovasc Med* 9: 839720, 2022. doi:10.3389/fcvm.2022.839720.
26. **Jablonski P**, **Howden BO**, **Rae DA**, **Birrell CS**, **Marshall VC**, **Tange J.** An experimental model for assessment of renal recovery from warm ischemia. *Transplantation* 35: 198–204, 1983. doi:10.1097/00007890-198303000-00002.
27. **Weekers L**, **de Tullio P**, **Bovy C**, **Poma L**, **Marée R**, **Bonvoisin C**, **Defraigne J-O**, **Krzesinski J-M**, **Jouret F.** Activation of the calcium-sensing receptor before renal ischemia/reperfusion exacerbates kidney injury. *Am J Transl Res* 7: 128–138, 2015.
28. **Chade AR**, **Tullos NA**, **Harvey TW**, **Mahdi F**, **Bidwell GL.** Renal therapeutic angiogenesis using a bioengineered polymer-stabilized vascular endothelial growth factor construct. *J Am Soc Nephrol* 27: 1741–1752, 2016. doi:10.1681/ASN.2015040346.
29. **Kim YG**, **Suga SI**, **Kang DH**, **Jefferson JA**, **Mazzali M**, **Gordon KL**, **Matsui K**, **Breiteneder-Geleff S**, **Shankland SJ**, **Hughes J**, **Kerjaschki D**, **Schreiner GF**, **Johnson RJ.** Vascular endothelial growth factor accelerates renal recovery in experimental thrombotic microangiopathy. *Kidney Int* 58: 2390–2399, 2000. doi:10.1046/j.1523-1755.2000.00422.x.
30. **Engel JE**, **Williams ML**, **Williams E**, **Azar C**, **Taylor EB**, **Bidwell GL**, **Chade AR.** Recovery of renal function following kidney specific VEGF therapy in experimental renovascular disease. *Am J Nephrol* 51: 891–902, 2020. doi:10.1159/000511260.
31. **Khbouz B**, **Rowart P**, **Poma L**, **Dahlke E**, **Bottner M**, **Stokes M**, **Bolen G**, **Rahmouni S**, **Theilig F**, **Jouret F.** The genetic deletion of the dual specificity phosphatase 3 (DUSP3) attenuates kidney damage and inflammation following ischaemia/reperfusion injury in mouse. *Acta Physiol (Oxf)* 234: e13735, 2021. doi:10.1111/apha.13735.
32. **Wever KE**, **Menting TP**, **Rovers M**, **van der Vliet JA**, **Rongen GA**, **Masereeuw R**, **Ritskes-Hoitinga M**, **Hooijmans CR**, **Warlé M.** Ischemic preconditioning in the animal kidney, a systematic review and meta-analysis. *PLoS One* 7: e32296, 2012. doi:10.1371/journal.pone.0032296.
33. **Pallet N**, **Thervet E**, **Timsit MO.** Angiogenic response following renal ischemia reperfusion injury: new players. *Progres en Urologie* 24, *Suppl* 1: S20–S25, 2014. doi:10.1016/S1166-7087(14)70059-4.
34. **Quarmby S**, **Kumar P**, **Wang J**, **Macro JA**, **Hutchinson JJ**, **Hunter RD**, **Kumar S.** Irradiation induces upregulation of CD31 in human endothelial cells. *Arterioscler Thromb Vasc Biol* 19: 588–597, 1999. doi:10.1161/01.atv.19.3.588.
35. **Sonveaux P**, **Brouet A**, **Havaux X**, **Grégoire V**, **Dessy C**, **Balligand J-L**, **Feron O.** Irradiation-induced angiogenesis through the up-regulation of the nitric oxide pathway: implications for tumor radiotherapy. *Cancer Res* 63: 1012–1019, 2003.
36. **Kozin SV**, **Duda DG**, **Munn LL**, **Jain RK.** Neovascularization after irradiation: what is the source of newly formed vessels in recurring tumors? *J Natl Cancer Inst* 104: 899–905, 2012. doi:10.1093/jnci/djs239.
37. **Ebos JML**, **Lee CR**, **Christensen JG**, **Mutsaers AJ**, **Kerbel RS.** Multiple circulating proangiogenic factors induced by sunitinib malate are tumor-independent and correlate with antitumor efficacy. *Proc Natl Acad Sci USA* 104: 17069–17074, 2007. doi:10.1073/pnas.0708148104.
38. **Norton K-A**, **Han Z**, **Popel AS**, **Pandey NB.** Antiangiogenic cancer drug sunitinib exhibits unexpected proangiogenic effects on

endothelial cells. *Onco Targets Ther* 7: 1571–1582, 2014. doi:10.2147/OTT.S65055.

39. **Neubig RR.** Mind your salts: when the inactive constituent isn't. *Mol Pharmacol* 78: 558–559, 2010. doi:10.1124/mol.110.067645.
40. **Geubelle P**, **Gilissen J**, **Dilly S**, **Poma L**, **Dupuis N**, **Laschet C**, **Abboud D**, **Inoue A**, **Jouret F**, **Pirotte B**, **Hanson J.** Identification and pharmacological characterization of succinate receptor agonists. *Br J Pharmacol* 174: 796–808, 2017. doi:10.1111/bph.13738.
41. **Chouchani ET**, **Pell VR**, **Gaude E**, **Aksentijević D**, **Sundier SY**, **Robb EL**, **Logan A**, **Nadtochiy SM**, **Ord ENJ**, **Smith AC**, **Eyassu F**, **Shirley R**, **Hu C-H**, **Dare AJ**, **James AM**, **Rogatti S**, **Hartley RC**, **Eaton S**, **Costa ASH**, **Brookes PS**, **Davidson SM**, **Duchen MR**, **Saeb-Parsy K**, **Shattock MJ**, **Robinson AJ**, **Work LM**, **Frezza C**, **Krieg T**, **Murphy MP.** Ischaemic accumulation of succinate controls reperfusion injury through mitochondrial ROS. *Nature* 515: 431–435, 2014. doi:10.1038/nature13909.